nature ecology & evolution

Article

https://doi.org/10.1038/s41559-025-02926-x

Intracellular interactions shape antiviral resistance outcomes in poliovirus via eco-evolutionary feedback

Received: 5 June 2025

Accepted: 31 October 2025

Published online: 05 December 2025

Check for updates

Alexander J. Robertson [1], Benjamin Kerr [2] ✉ & Alison F. Feder [3,4,5] ✉

Resistance evolution can undermine antiviral treatment. However, targeting antivirals to shared viral proteins could inhibit resistance evolution if susceptible viruses sensitize resistant ones during cellular coinfection. Pocapavir, a poliovirus capsid inhibitor, uses this sociovirological interference strategy. While susceptible viruses substantially suppress pocapavir resistance in cell culture, a pocapavir clinical trial found widespread resistance and limited clearance time improvements in treated participants. Here, to reconcile these findings, we present an intrahost eco-evolutionary model of pocapavir-treated poliovirus, which reproduces both in vitro interference and clinical resistance evolution. In the short term, high densities of susceptible viruses sensitize resistant ones, mirroring cell culture results. However, over multiple replication cycles, pocapavir's high potency collapses viral density, reducing coinfection and enabling resistance evolution, as observed clinically. Because resistance suppression relies on coinfection, enhancing susceptible virus survival could offer therapeutic advantages. Counterintuitively, we demonstrate that lessening antiviral potency can increase coinfection, limiting resistance while also maintaining low viral load. These findings suggest that antivirals relying on viral intracellular interactions must balance immediate neutralization with preserving future coinfection for sustained inhibition. Explicitly considering the eco-evolutionary feedback encompassing viral density, shared phenotypes and absolute fitness provides new insights for effective therapy design and illuminates viral evolutionary dynamics more broadly.

Resistance evolution can undermine otherwise successful antimicrobial treatments if drug application permits microorganisms carrying resistance alleles to expand and prevent population extinction. Implicit in these dynamics is that selection for phenotypic resistance also selects genotypic resistance, which permits the trait to carry forward into future generations. While such an assumption is often valid in bacterial populations[1,2] (Fig. 1a–c), in viruses, the association between genotype and phenotype can be more complicated[3–5]. For example, both cellular coinfection and de novo mutation during viral replication can result in distinct genotypes occupying the same cell. These genotypes may share intracellular protein products, and as a result, a particular genotype may be associated, fully or partially, with the protein products of a different genotype[6] (Fig. 1d,e).

This so-called phenotypic mixing has important implications for resistance evolution[5,7]. First, the disassociation between genotype and phenotype can impair selection for resistant genotypes. Consider a cell

[1]Molecular and Cellular Biology Graduate Program, University of Washington, Seattle, WA, US. [2]Department of Biology, University of Washington, Seattle, WA, US. [3]Department of Genome Sciences, University of Washington, Seattle, WA, US. [4]Herbold Computational Biology Program, Fred Hutchinson Cancer Center, Seattle, WA, US. [5]Howard Hughes Medical Institute, Seattle, WA, US. ✉e-mail: kerrb@uw.edu; affeder@uw.edu

https://doi.org/10.1038/s41559-025-02926-x

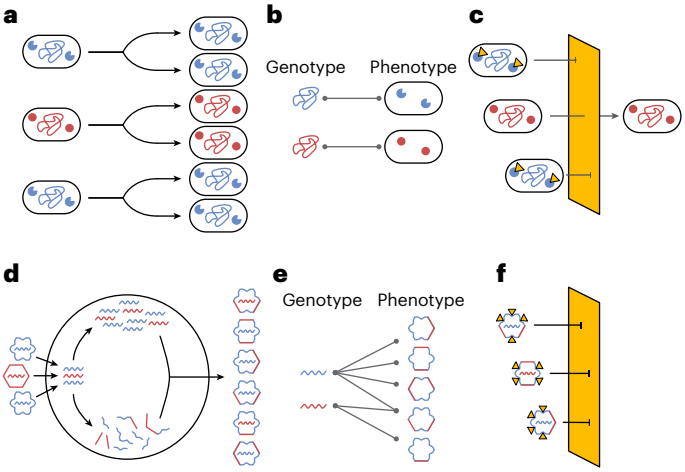

Fig. 1 | Genotype–phenotype disassociations can limit resistance evolution. **a**, In bacterial populations, resistance-conferring genotypes exist at low frequencies before treatment. **b**,**c**, Because genotypes are directly associated with the phenotypes they encode (**b**), drug application that selectively favours the survival of resistant phenotypes drives the expansion of resistant genotypes (**c**). **d**, In viruses, multiple genotypes (that is, resistant and susceptible) may coinfect the same cell via mutation or superinfection and the protein products they encode can mix intracellularly. **e**,**f**, The resulting chimeric phenotypes can be associated with either genotype (**e**), and even those phenotypes that are partially composed of resistant proteins may be susceptible to drug neutralization (**f**). Throughout the figure, red and blue represent resistant and susceptible variants, respectively, and yellow triangles represent antimicrobials that can bind to susceptible proteins.

that contains both treatment-resistant and susceptible genotypes. If resistant genotypes do not associate with resistant protein products, those genotypes may not survive drug application, limiting their contribution to future generations (Fig. 1f). Second, phenotypic mixing can limit the creation of resistant phenotypes themselves. If a drug targets an oligomeric protein product (for example, a capsid inhibitor that targets the capsid), susceptible proteins can act in a dominant negative fashion to interfere with the phenotypic expression of resistance. Capsid inhibitors may neutralize chimeric capsids composed of both susceptible and resistant subunits if enough susceptible subunits are available to bind the drug. If intracellular resistant genotypes are rare (such as after de novo mutation of a resistant mutant), cells may produce few or no phenotypically resistant capsids. The presence of one or both of these factors could present an opportunity to treat viral infections while muting selection for resistance.

Exploiting phenotypic mixing to suppress resistance evolution while treating viral infections partially underlies the promise of the poliovirus capsid inhibitor pocapavir[6,8]. Pocapavir strongly inhibits poliovirus, but mutations in the genes encoding capsid subunits VP1 or VP3 disrupt drug binding and confer resistance[9,10]. When resistant viruses are cocultured with susceptible ones and treated with pocapavir, resistant genomes are packaged in chimeric resistant-susceptible capsids and are neutralized by the drug[6]. As a result, cocultured resistant viruses have substantially reduced viral titres compared with resistant viruses grown in isolation (Fig. 2a). Promisingly, pocapavir was used to slow disease progression in vivo in poliovirus-infected mice with no detected resistance evolution[6]. However, in a larger placebo-matched human clinical trial in which participants received the live attenuated polio vaccine and were treated with pocapavir, the drug both failed to significantly reduce the time to viral clearance in three of four placebo-matched groups and led to resistance in nearly half of pocapavir-treated participants[11] (Fig. 2b). While a subset of pocapavir recipients did clear their virus early without apparent resistance evolution (and pocapavir therapy has been successfully used in certain compassionate use cases[12,13]), results from the clinic have been mixed, and, to our knowledge, have not led to additional trials. More generally, this study raises doubts about the therapeutic potential of exploiting phenotypic mixing.

To investigate these conflicting findings, we developed a dynamical model of poliovirus replication and evolution under drug treatment. Surprisingly, we find that a single model can reproduce the seemingly contradictory in vitro cell culture and clinical results via its behaviour at different viral densities. At high viral density, susceptible viruses mask the phenotype of resistant ones and suppress selection for resistance, as observed in cell culture. However, as successful treatment drives the viral density down, limited intracellular viral interaction restores the standard genotype–phenotype association. At this point, resistant and susceptible genomes associate strongly with their own phenotype, and drugs can efficiently select for genotypic resistance. Counterintuitively, this suggests that, in our model, permitting more susceptible viruses to survive drug application can better suppress resistance evolution and lead to smaller viral population sizes over time. This study provides a theoretical framework for evaluating viral evolutionary responses to therapies targeting resistance phenotypes encoded by multiple genotypes, serves as a guide for the development of novel antimicrobials and dosing strategies, and highlights the importance of emergent dynamical responses when exploiting virus–virus interactions in medicine.

Results

Poliovirus eco-evolutionary model

We developed a discrete-generation dynamical model that tracks poliovirus genotypes and phenotypes over multiple rounds of viral replication and analysed the model using deterministic and stochastic simulations (Methods; see Extended Data Table 1 for parameters). In brief, each generation consists of four steps (Fig. 3a):

(1) Viral entry into host cells: resistant and susceptible genomes enter cells as a function of their respective population sizes. Coinfection is more likely if viral population sizes are large relative to the host cell population.
(2) Genome replication and mutation: intracellular viral genomes replicate up to the cell's burst size. Mutation can interconvert resistant and susceptible genotypes.
(3) Capsid formation: initial infecting genomes produce a pool of shared capsid subunits. For mixed infections, capsids are formed by randomly drawing 60 subunits from this pool and can be composed of both resistant and susceptible subunits.
(4) Capsid packaging: newly replicated viral genomes are packaged into assembled capsids in proportion to their intracellular abundances.

Viruses then exit cells and pocapavir can bind and neutralize free virions according to their capsid phenotype. We parametrized viral neutralization rates based on the reduction in viral titres measured experimentally in pocapavir-treated populations of mixed resistant and susceptible cultures (see 'Parameter inference' section in the Methods). Capsids composed solely of resistant subunits survive pocapavir application with probability 1, while those composed of fully susceptible subunits survive with probability 4×10^{-4} (Fig. 3b). Our model recapitulates the observations of Tanner et al.[6] that titres of resistant viruses (specifically, viral genomes encoding resistant subunits) decrease when coinfected alongside susceptible viruses when treated with pocapavir (Fig. 3c,d).

Resistance suppression is dependent on susceptible virus density

We first assessed the conditions under which pocapavir resistance evolution is suppressed during a single round of replication with pocapavir treatment. Specifically, we measured the change in resistance

https://doi.org/10.1038/s41559-025-02926-x

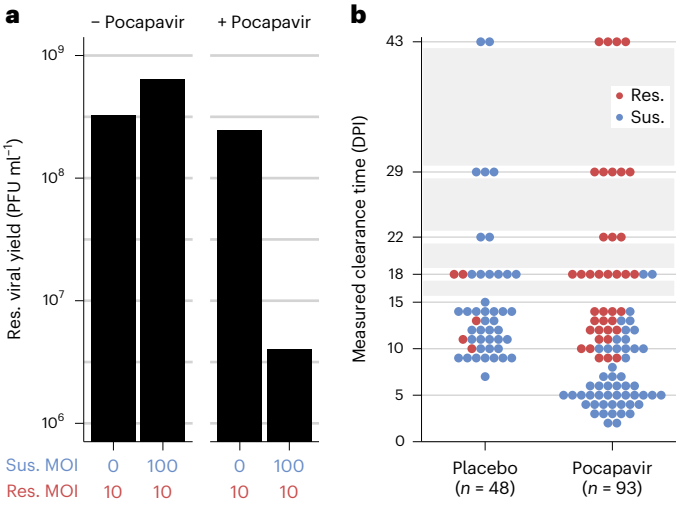

Fig. 2 | Pocapavir-treated poliovirus outcomes diverged between cell culture and clinical trial settings. a, In vitro experiments by Tanner et al.[6] demonstrated that coinfection of drug-resistant (res.) and susceptible (sus.) poliovirus strains suppresses the yield of resistant virus under pocapavir treatment. **b**, In the clinical trial reported by Collett et al.[11], pocapavir failed to significantly reduce time to infection clearance compared with a placebo in three of four matched groups of participants administered the live attenuated poliovirus vaccine, and resistance was enriched in the pocapavir group. Points represent the clearance dates of individual trial participants and are coloured by resistance status (resistance in red, susceptible in blue), and grey boxes indicate dates that were not sampled during the trial (DPI, days post infection).

frequency as a function of the total multiplicity of infection (MOI—viral density, defined as the ratio of the total number of viruses to the total number of infectable host cells). We initialized simulations with the resistant genotype frequency set at $f_{Res} = 10^{-4}$, consistent with levels observed in untreated poliovirus populations[6,10].

At high MOIs (MOI ≈ 10^2), genotypic resistance increased in frequency by less than 10^{-3} after a single round of replication in the presence of pocapavir (Fig. 4a). These results are consistent with Tanner et al.[6] and the logic underlying phenotypic mixing. However, this resistance suppression did not extend to populations that were initialized at lower MOIs. At MOI ≤1, the resistant genotype frequency increased to more than 12% of the population in a single round of replication. These results can be understood in the context of the MOI controlling the degree of coinfection and subsequently the strength of the genotype–phenotype association. At high MOIs, coinfection is ubiquitous and rare genotypes are not often associated with their capsid phenotype (Fig. 4b and Extended Data Fig. 1). However, at low MOIs, coinfection is rare and genotypes and phenotypes associate directly (Fig. 4c), allowing resistant genotypes to directly benefit from their encoded phenotype without interference.

We next considered that infections are dynamic processes, and the degree of viral suppression or proliferation in one generation may determine viral density in subsequent generations. If pocapavir treatment drastically reduces the viral density (and consequently the total MOI), this may lead to conditions in which resistance can emerge. We therefore performed an in silico serial passaging experiment in which we inoculated cell populations at a high MOI (MOI of 100) with predominantly susceptible viruses (resistant genotype frequency $f_{Res} = 1 \times 10^{-4}$). We allowed viruses to replicate and be neutralized by pocapavir, and seeded the surviving viruses on fresh cell populations over multiple generations.

Consistent with single-step experiments at high MOI, the viral population decreased in abundance after one round of replication in the presence of pocapavir (Fig. 4d). As a result, the surviving viral progeny infected cells at substantially reduced MOI and resistant genomes increased in both frequency and abundance after a second and third round of passaging. Once the viral population had recovered enough for widespread coinfection, resistant genotypes outnumbered susceptible ones over 100-fold, and susceptible subunits no longer sensitized their resistant counterparts (Extended Data Fig. 2). Rather, resistant viruses appeared to shield rare susceptible genomes in a form of socially encoded cross protection. These dynamics can be understood by tracking the change in MOI and resistance frequency on a stepwise phase diagram, initiating simulations across a range of initial total MOIs and resistance frequencies (Fig. 4e). Initial conditions with low resistance frequencies and sufficiently high MOI lead first to a rapid reduction in the MOI, which then permits increases in the genotypic frequency of resistance. Note that one way to interpret this sequence is that the low viral titre output in Fig. 4b is the low MOI input in Fig. 4c, enabling the spread of resistant viruses. Regardless of the initial conditions in our deterministic model (MOI > 0, $f_{Res} \in [0,1]$), resistance becomes the dominant genotype over time. Despite phenotypic mixing effectively suppressing resistance at high MOIs, rapid population contraction in response to pocapavir ultimately undermines that suppression.

Stochastic model replicates clinical trial outcomes

While our deterministic model can explain how resistance to pocapavir may have emerged in clinical trial participants despite phenotypic mixing, it cannot recapture the clinical trial observation that a subset of pocapavir recipients clear their infections early with little to no resistance evolution[11] (Fig. 2b). To investigate the dynamics driving the clinical trial clearance times, we implemented a stochastic version of the model in which simulated viral elements were drawn from probability distributions at each replication step in a finite host cell population with

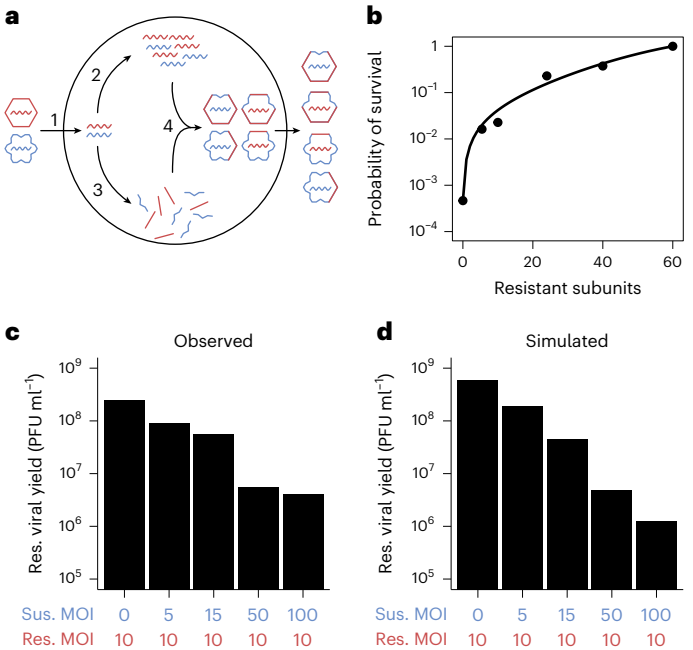

Fig. 3 | Discrete-time model of poliovirus replication, mutation and survival under pocapavir treatment. a, We simulate intracellular poliovirus dynamics in four stages: (1) viral entry into host cells, (2) genome replication with mutation, (3) production of capsid subunits and (4) assembly and packaging of progeny virions. **b**, Capsid-mediated survival is modelled by culling progeny virions according to their capsid composition. Capsid survival probability as a function of the number of resistant subunits (line) was fitted from cell culture experimental data from Tanner et al.[6] (points). **c**,**d**, Resistant viral yield under different intensities of susceptible virus coinfection shows a density-dependent effect in vitro[6] (**c**) and in silico under our model (**d**). Throughout the figure, resistant variants are illustrated in red and susceptible variants are illustrated in blue.

https://doi.org/10.1038/s41559-025-02926-x

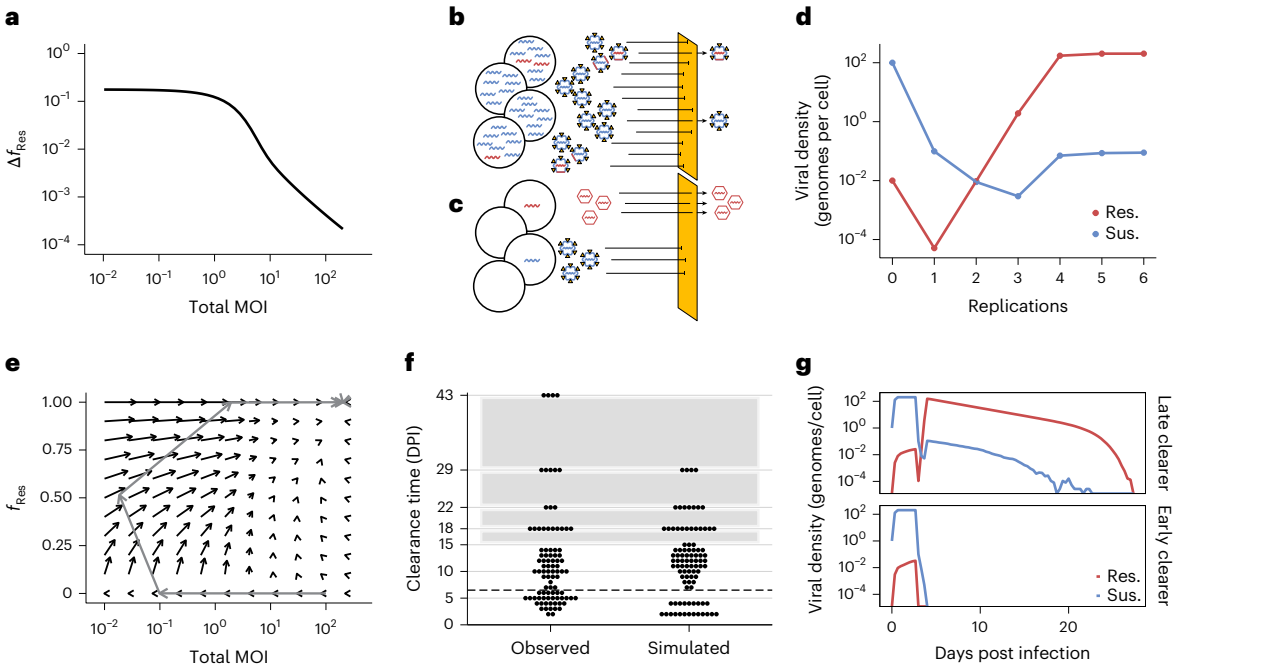

Fig. 4 | Resistance suppression is MOI dependent, and resistance emerges if bottlenecks do not lead to extinction. a, Change in resistance frequency in a single generation (Δf_{Res}) depends on the MOI (initial $f_{Res} = 1 \times 10^{-4}$). **b**, At high MOI, rare resistant genomes are encapsidated by phenotypically susceptible capsids, muting genotypic selection. Although nearly all capsids are phenotypically susceptible, some survive pocapavir administration (a fraction greatly exaggerated for this cartoon), as observed in cell culture. **c**, At low MOI, viruses singly infect cells, and rare resistant genomes are encapsidated by phenotypically resistant capsids, enabling selection for resistance. **d**, Over multiple generations, pocapavir treatment transiently reduces viral population size for both resistant and susceptible genomes but leads to viral rebound of a primarily genetically resistant population following low population density. **e**, The discrete step phase diagram shows the joint change in genotypic resistance frequency and MOI from different initial conditions. Arrows are shortened by 80% to increase legibility. The trajectory from **d** is overlaid in grey. **f**, Clearance dates from the observed clinical trial and one simulated clinical trial of $n = 93$ viral populations treated with pocapavir. The dashed line indicates the date of the earliest placebo clearance. **g**, Late and early clearers both experienced drops in resistant and susceptible viral population size with diverging outcomes following the population bottleneck. Throughout the figure, resistant variants are illustrated in red and susceptible variants are illustrated in blue.

an immune system that responds to infection (see 'Immune clearance' section in the Methods). In brief, we modelled viral immune clearance via a non-specific, ramping innate immune response that removes viruses irrespective of capsid phenotype and parameterized clearance rate and host cell population size based on the clearance dates in the clinical trial placebo group. We used this model to simulate an in silico pocapavir clinical trial by running 93 simulations (representing 93 trial participants) until viral extinction. The infections were initialized with one susceptible virus per host cell and no resistant viruses. Pocapavir was administered after 24 h (three rounds of replication, $n = 23$) or 72 h (nine rounds of replication, $n = 70$), as in the clinical trial.

Our model broadly recaptures the clearance time and resistance evolution outcomes observed by Collett et al.[11]. Specifically, viral populations exhibit a bifurcation of outcomes, in which they clear shortly after pocapavir initiation (<7 days after infection) with little genotypic resistance, or clear later (≥7 days after infection) with widespread genotypic resistance (Fig. 4f). Analysis of the simulated population trajectories revealed that both early clearers and late clearers experienced sharp population bottlenecks and low MOIs shortly after pocapavir initiation (Fig. 4g and Extended Data Fig. 3). In late clearers, this bottleneck allowed for rapid, resistance emergence according to the dynamics explored above, whereas in early clearers, this bottleneck led to stochastic extinction. Repeating clinical trials with different host cell population sizes led to changes in the relative probabilities of these two outcomes (Extended Data Fig. 4), but not their qualitative behaviour.

Collett et al.[11] also observed that a greater proportion of participants treated at 24 h exhibited resistance than the 72-h treatment group (15/23 versus 25/70, Fisher's exact test, $P = 0.0163$), which is potentially unexpected given that more resistant genomes are expected to exist after 72 h. Under certain starting conditions in our model, this pattern can emerge because resistant genomes produced before widespread coinfection can be more tightly linked to their resistant phenotype, counterbalancing their lower numbers (Extended Data Fig. 5). In sum, our model can explain counterintuitive and divergent participant outcomes among pocapavir recipients in observed by Collett et al.[11].

Resistance cost, but not dominance effects, can change simulation outcomes

We tested whether variations of the fitness function—either imposing a fitness cost of resistance or altering the phenotypic dominance of resistant subunits (that is, the number required to confer drug survival)—affected our results. Introducing a resistance cost slowed resistance evolution, reduced equilibrium resistance and increased stochastic clearance during bottlenecks (Extended Data Fig. 6). However, this effect may not be clinically relevant, as pocapavir resistance mutations do not appear costly in cell culture[6,9,10]. By contrast, varying dominance had no qualitative effect on resistance outcomes (Extended Data Fig. 7 and Supplementary Text 1).

Reduced drug potency can enhance long-term control of resistance and lower viral burden

The critical liability of pocapavir identified above is that effective neutralization of the virus disrupts susceptible viruses' abilities to interfere with resistant phenotypes via coinfection. We hypothesized that increased survival of susceptible viruses would enhance resistance suppression by maintaining higher rates of coinfection over time. Furthermore, because high viral loads follow resistance emergence, suppressing resistance could reduce total burden despite survival of susceptible viruses. We

https://doi.org/10.1038/s41559-025-02926-x

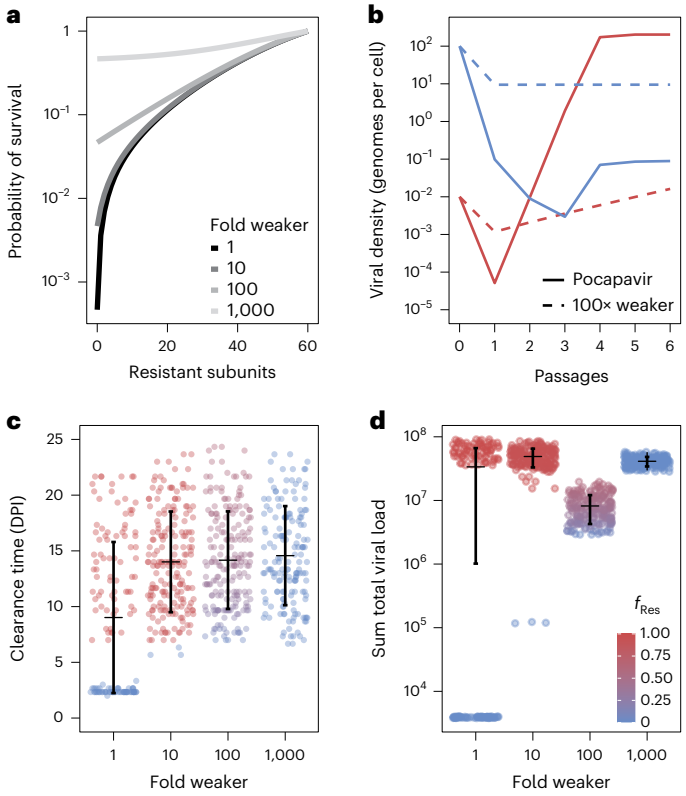

Fig. 5 | Drugs less potent than pocapavir can better suppress resistance and maintain lower viral loads. a, We modelled hypothetical drugs 10×, 100× and 1,000× weaker than pocapavir and plot the probability of virion survival as a function of the number of resistant capsid subunits under these drug conditions. **b**, In deterministic serial passage experiments, the 100× weaker drug maintained a lower total viral population than pocapavir (resistant genomes, red; susceptible genomes, blue). We simulated clinical trials of individuals treated with drugs 1×, 10×, 100× and 1,000× weaker than pocapavir. **c**,**d**, Reducing drug potency delayed mean clearance time measured by days post infection (**c**) but had a non-monotonic effect on the sum viral load over the course of the infection (**d**) ($n = 100$ for each group). In both **c** and **d**, dots represent individual simulations and are coloured based on the frequency of resistance in the population over the course of the infection (scale in **d**). Error bars show the mean (black dash) ± variance. For an expanded range of drug potencies, see Extended Data Fig. 8b,c.

therefore considered the effects of hypothetically less potent drugs (or alternatively, lower doses of pocapavir) that permitted greater degrees of survival by virions with fully or partially susceptible capsids (Fig. 5a; see 'Variation in drug strength' section in the Methods).

Reducing drug potency led to smaller gains in resistant genotype frequency in a single round of replication, in line with evolutionary expectations for weaker selective pressures (Extended Data Fig. 8a). However, reducing drug efficacy also led to a less rapid decline in the absolute number of susceptible genomes. For example, a drug with a 100-fold reduced efficacy reduced the MOI after a single generation to approximately 10, whereas pocapavir reduced the MOI to substantially less than one virus per cell (Fig. 5b). As a result of this sustained moderate MOI, genotypic resistance increased minimally (up to 0.16% of the population) over the next six passages while genotypic resistance under pocapavir reached near 100%. Because resistance remained suppressed, the population did not undergo full viral rebound and the total MOI after six passages was approximately 20 times smaller under the 100× less potent drug than pocapavir. This suggests that reducing antiviral potency can, under some circumstances, improve multiple aspects of viral control.

To evaluate the potential clinical implications of reducing antiviral potency, we simulated in silico clinical trials of 100 individuals treated with reduced potency drugs (Fig. 5c,d, assessed across a greater range in Extended Data Fig. 8b,c). We found that pocapavir had an earlier mean clearance time compared with the less potent hypothetical drugs. Reduced drug potency weakened population bottlenecks, preventing stochastic extinction of viral populations at small population sizes when treated with drugs weaker than pocapavir.

By contrast, reducing drug potency had more complex effects on the frequency of resistance and the sum total viral population size over the course of infection (Fig. 5d). Reducing drug potency by a factor of 10 resulted in near ubiquitous resistance evolution and high viral population sizes across trial participants. This reflects that a 10× reduced potency is a strong enough selective pressure to bring viral populations into a regime in which cells are singly infected and resistance can evolve, but does not cause the severe bottlenecks and stochastic extinctions seen with pocapavir. By contrast, reducing drug potency by a factor of 100× produced sufficiently gradual viral decay during initial drug application to allow resistant-susceptible coinfection to be durably maintained. While this rate of viral decay was not strong enough to cause stochastic extinction during bottlenecks, the sustained coinfection reduced the rate of resistance evolution and subsequently the total viral load compared with pocapavir. Finally, a very strong reduction of drug potency by a factor of 1,000× selected for almost no resistance evolution, but also did not restrict the viral population relative to an untreated control. This suggests that, while reducing drug potency can improve multiple important clinical metrics within the context of our model, not all reductions in drug potency will have favourable effects and there is an optimal balance between preserving susceptible virus and limiting total infection burden.

Discussion

In this Article, we show that a single model of poliovirus population dynamics and genetics can reconcile seemingly divergent outcomes of pocapavir treatment in cell culture[6] and clinical trial settings[11]. Our key insight is that therapeutic strategies that rely on interaction between viruses must account for the demographic effects of therapeutic success. If the long-term efficacy of these therapies depends on the durability of intracellular interactions, lowering viral density through successful treatment can decrease coinfection rates and thus the potential for therapeutically beneficial interactions between viral genomes and their encoded proteins.

There is growing interest in exploiting interactions between viral genomes for therapy. Most efforts rely on defective genomes that parasitize replication-competent viruses rather than on sensitization mechanisms like those we model here[14–16]. Perhaps the most promising of these strategies are therapeutic interfering particles (TIPs—replication-incompetent mutants that suppress replication-competent viruses during coinfection), because their interference can strengthen as their population grows. Although TIPs are an active area of investigation, Pitchai et al.[17] recently demonstrated an effective proof of concept for using TIPs to treat human immunodeficiency virus over short timescales. The demographic feedback considered in our model highlights potential challenges with such an approach; over longer periods of time, if TIPs drive replication-competent viruses to near but not complete eradication, TIPs may lose their ability to self-renew and themselves become eliminated. This could ultimately lead to the unencumbered rebound of replication-competent viruses, especially in the case of a virus such as human immunodeficiency virus that can reactivate from a latent reservoir after TIPs have been eliminated.

If intracellular interactions are crucial for the success of these treatments, how can they be maintained in the face of demographic collapse? In the case of TIPs, Weinberger, Schaffer and Arkin[15] found that weaker interference between TIPs with their wild-type counterparts favours the long-term success of TIP therapy[15]. Indeed, all successful demonstrations of TIPs in rodents[18–20] or mosquitoes[20] allow sufficient wild-type replication to maintain therapeutic pressure in subsequent

https://doi.org/10.1038/s41559-025-02926-x

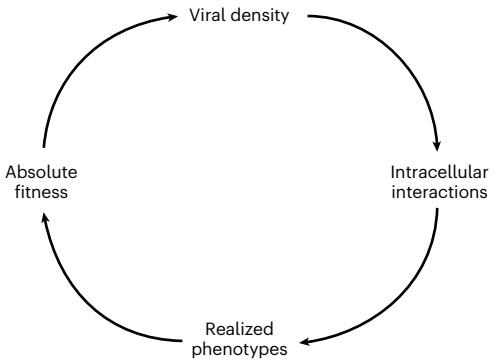

Fig. 6 | Targeting viral traits affected by multiple intracellular viral genomes requires an understanding of eco-evolutionary feedback. Viral density determines the degree of intracellular interactions, which in turn shapes realized phenotypes, influencing absolute fitness, which then feeds back into viral density in the next generation.

generations. In our model of poliovirus and pocapavir, we achieve sustained intracellular interaction through a similar therapeutic intervention—decreasing drug intensity. Modifying drug intensity through dosage or administration frequency may allow more fine-tuned calibration of intracellular interactions than identifying TIPs with the appropriate degree of interference. To be clear, this is not a clinical recommendation, and many important model assumptions would need to be rigorously evaluated in experimental settings before altering any therapeutic approach. However, similar strategies to prolong drug efficacy by exploiting interactions between different genotypes are also being explored in non-virology settings. For example, in drug-treated bacterial[1,2] and cancer[21,22] populations, moderate-dose or pulsed strategies can prolong competition between susceptible and resistant cells, thereby lowering the overall population size over time and delaying treatment failure.

Although these treatment strategies reckon with similar demographic dynamics presented here, they may require different medical and public health considerations. For example, managing disease severity and resistance evolution without eliminating the replicating population may be acceptable in cancer treatment; however, prolonged infections could lead to more opportunities for disease spread in the case of a transmissible pathogen. Furthermore, although we focused on virus–virus interactions causing interference in this study, there are other instances where these interactions may be beneficial[4,7,23–26] (Supplementary Text 2). When considering viral evolution in these settings, models that bridge intra- and interhost dynamics, and consider positive demographic feedback loops, could be valuable.

A central assumption in our model is that the number of viruses per host cell is the primary driver of coinfection rate. While this assumption is common[4,27–29], diverse viral behaviours can modulate coinfection. For example, the first virus infecting a cell can prevent others from entering in a process called superinfection exclusion[30]. Conversely, en bloc transmission, in which viruses are packaged and transmitted collectively, can enhance coinfection[31,32]. To our knowledge, poliovirus does not exhibit superinfection exclusion[33,34], but growing evidence suggests that en bloc transmission[31,32,35] and even shuttling of poliovirus by enteric bacteria[36] can be common during infection. These factors could elevate poliovirus coinfection rates beyond what we consider in our model, or change which genotypes coinfect together.

Host and environmental factors could also affect the realized frequency of coinfection and subsequent evolutionary dynamics. We assume that cells are equally susceptible to poliovirus infection and spatially well mixed. In practice, expression of poliovirus' primary receptor, CD155, varies considerably among cells[37] and at different stages of disease[38]. This could concentrate virus into a smaller number of cells, enhancing interference, or result in certain cells that can only be infected by few virions, potentially allowing greater expression of phenotypic resistance. The organization of host cells in a tissue also stands to impact coinfection dynamics[39]. Limited viral dispersal could increase coinfection and therefore interference, but it might also concentrate resistant genomes into the tissue sections in which they initially arose, limiting the degree to which susceptible genomes could interfere with resistant spread. This effect might also vary across organ systems. Notably, the limited resistance evolution observed in pocapavir-treated mice may relate to increased viral density in neuronal infections[6,40] relative to the gut epithelial infections of the pocapavir clinical trial in which resistance evolution was common. Investigating the importance of intrahost spatial and environmental variation is an important future area of research.

A second potentially important form of spatial organization is intracellular. Many viruses, including poliovirus, form membrane-associated structures that can sequester viral components near their encoding genomes[41,42]. This effect could limit protein diffusion and reduce phenotypic mixing. Poliovirus capsids are tethered to their membranes during virion assembly[43], so it is possible that some degree of intracellular segregation contributes to our observation that even very rare resistant genomes in a cell impart partial phenotypic resistance. Despite this, Tanner et al.[6] observed that phenotypically distinct capsid proteins intermingle in single chimeric virions, so the exact extent of intracellular mixing of poliovirus capsid subunits remains unknown. Nevertheless, the organization of viruses within a cell is likely to be a key determinant of therapeutic strategies built around intracellular resource sharing.

More broadly, our study contributes to a growing body of work framing viral coinfection through the lens of ploidy, drawing parallels to how multiple gene copies shape phenotype in cellular organisms[7,44–46]. In classical diploid genetics, a single biallelic locus can produce up to three phenotypes, depending on the interactions between the alleles (that is, the 'dominance' of one allele over the other). Although the frequency of these phenotypes can shift between generations, the ploidy level itself remains fixed. Among viruses, the number of genomes that contribute to a phenotype can vary between host cells and dynamically over the course of an infection[7]. The association of several viral genomes in a host cell can lead to more complex and varied phenotypes than is possible in a diploid model[47]. The model that we explore here has a classical analogue to incomplete dominance in a standard diploid framework, in which the addition of more resistant proteins always partially benefits a capsid in the presence of the drug. However, recent work has also described instances of apparent over- or underdominance in which coinfecting viruses have increased or decreased fitness relative to non-mixed infections[48–51]. Regardless of the exact form of intracellular dominance, shared phenotypes can clearly determine viral fitness. Because absolute fitness within a population governs viral density in the immediate future, it therefore impacts the degree of viral intracellular interaction moving forward, and thus how new phenotypes are realized. Therefore, viral 'ploidy' not only changes over time, but feeds back into itself (Fig. 6). Although our model centres on poliovirus and pocapavir, its core principles—density-driven coinfection, transient genotype–phenotype associations and demographic feedback with the environment—are likely to be broadly relevant for designing therapies that exploit the social lives of viruses, as well as viral evolutionary dynamics more broadly.

Methods

We developed both stochastic and deterministic versions of a discrete-time dynamical model of poliovirus replication that integrates viral entry, genome replication, mutation, capsid formation, pocapavir neutralization and immune clearance. We describe the stochastic version here, while the deterministic version follows the same probability distributions but accounts for every possible outcome (that is,

integrates over the distribution) rather than drawing specific values. Full details are provided in the Supplementary Materials and Methods. All simulations and analyses were performed in R, version 4.1.0[52]. Data visualization was performed with the ggplot2 package[53].

Viral entry

At time t, the total viral population, $v_{\mathrm{tot},t}$, consists of $r_{\mathrm{tot},t}$ resistant and $s_{\mathrm{tot},t}$ susceptible genomes, yielding

$$v_{\mathrm{tot},t} = r_{\mathrm{tot},t} + s_{\mathrm{tot},t}.$$

We assume that viruses are equally likely to infect any of the γ host cells in the population, and that there is no superinfection exclusion. The number of resistant and susceptible genomes entering a cell (random variables R_{inf} and S_{inf}, respectively) are modelled by binomial distributions,

$$R_{\mathrm{inf}} \sim \mathrm{Bin}\left(r_{\mathrm{tot},t}, \frac{1}{\gamma}\right) \qquad S_{\mathrm{inf}} \sim \mathrm{Bin}\left(s_{\mathrm{tot},t}, \frac{1}{\gamma}\right), \tag{1}$$

where ~ means 'is distributed as'. The total number of viruses that have infected a given cell, v_{inf}, can be described by the equation $v_{\mathrm{inf}} = r_{\mathrm{inf}} + s_{\mathrm{inf}}$, where r_{inf} and s_{inf} represent realizations of the binomial distributions described in equation (1). Thus, on average, v_{inf} will equal $\frac{v_{\mathrm{tot},t}}{\gamma}$, the MOI.

We note that, in the deterministic model, $r_{\mathrm{tot},t}$ and $s_{\mathrm{tot},t}$ need not be integers, rendering the binomial distribution undefined. We describe a weighted sampling scheme to circumvent this issue in the 'Viral entry' section in the Supplementary Materials and Methods.

Genome replication and mutation

For each infected cell, progeny production (V_{rep}) follows a Poisson distribution with a mean of the inferred average effective burst size, β, which accounts for the number of infectious particles that leave the cell (that is, V_{rep} ~ Pois(β) for $v_{\mathrm{inf}} > 0$). Replicated resistant genomes (R_{rep}) are modelled as

$$R_{\mathrm{rep}} \sim \mathrm{Bin}\left(v_{\mathrm{rep}}, \frac{r_{\mathrm{inf}}}{v_{\mathrm{inf}}}\right).$$

Given that R_{rep} takes on some value, r_{rep}, the number of newly replicated susceptible genomes in a cell, s_{rep}, is given by

$$s_{\mathrm{rep}} = v_{\mathrm{rep}} - r_{\mathrm{rep}}.$$

Mutation between genotypes occurs per replication event at rate $\mu = 2 \times 10^{-5}$ (ref. 9), so that resistant and susceptible mutants (the random variables R_{mut} and S_{mut}, respectively) are found by

$$R_{\mathrm{mut}} \sim \mathrm{Bin}\left(s_{\mathrm{rep}}, \mu\right) \quad \text{and} \quad S_{\mathrm{mut}} \sim \mathrm{Bin}\left(r_{\mathrm{rep}}, \mu\right).$$

Given that R_{mut} and S_{mut} take on the values r_{mut} and s_{mut}, respectively, post-mutation genome counts per cell (r_{pool} and s_{pool}) are then found as follows:

$$r_{\mathrm{pool}} = r_{\mathrm{rep}} - s_{\mathrm{mut}} + r_{\mathrm{mut}}, \quad s_{\mathrm{pool}} = s_{\mathrm{rep}} - r_{\mathrm{mut}} + s_{\mathrm{mut}}.$$

Capsid formation

Let σ represent the number of subunits in a capsid. Each progeny genome is packaged into a capsid composed of 60 subunits ($\sigma = 60$). The number of resistant subunits per virion (the random variable I) is modelled binomially, where

$$I \sim \mathrm{Bin}\left(\sigma, \frac{r_{\mathrm{inf}}}{v_{\mathrm{inf}}}\right),$$

assuming that both resistant and susceptible genomes contribute equally to the pool of capsid subunits. The probability that a capsid has i resistant subunits is

$$p_i = \Pr(I = i | \{v_{\mathrm{inf}}, r_{\mathrm{inf}}\}),$$

where i takes on a discrete value between 0 and σ inclusive.

Genomes are assigned to capsids via a multinomial sampling process for each infected cell in the population. The number of replicated resistant genomes that are packaged into a capsid with i resistant subunits is the random variable $R_{\mathrm{pack},i}$. Each $R_{\mathrm{pack},i}$ can be collected into a vector R_{pack}, where

$$R_{\mathrm{pack}} \sim \mathrm{Multinom}(r_{\mathrm{pool}}, p_0, \ldots, p_\sigma)$$

with analogous sampling for susceptible genomes. At this point, virions leave their cells and are pooled into groups according to their capsid subunit composition and genotype.

Pocapavir neutralization

Drug neutralization is modelled by assigning each virion a survival probability, $\omega(i, t)$, that depends on its capsid composition (number of resistant subunits i) and on the time of drug administration t_{poc}. For $t < t_{\mathrm{poc}}$, $\omega(i, t) = 1$ (that is, before drug application, virions are not affected by the drug). When $t \geq t_{\mathrm{poc}}$, survival is given by a scaled logistic function:

$$\omega(i, t) = y_0 + (y_\sigma - y_0) \times \frac{L(i) - L(0)}{L(\sigma) - L(0)},$$

where $L(i)$ is the standard form of the logistic function:

$$L(i) = \frac{1}{1 + \mathrm{e}^{-k(i - i_0)}}.$$

The variables y_0 and y_σ represent the survival probabilities of fully susceptible and fully resistant capsids, respectively, and k and i_0 are inferred by fitting the function to cell culture survival probabilities from Tanner et al.[6]. Under drug pressure, the survival of virions carrying resistant genomes (the random variable $R_{\mathrm{surv},i}$) is then found by binomial sampling $r_{\mathrm{pack},i}$:

$$R_{\mathrm{surv},i} \sim \mathrm{Bin}\left(r_{\mathrm{pack},i}, \omega(i, t)\right),$$

for each capsid subunit state (and similarly for susceptible virions). $R_{\mathrm{surv},i}$ then takes on the specific values $r_{\mathrm{surv},i}$. After pocapavir neutralization, the total number of resistant genomes, r_{sum}, is calculated by summing across all $r_{\mathrm{surv},i}$:

$$r_{\mathrm{sum}} = \sum_{i=0}^{\sigma} r_{\mathrm{surv},i}.$$

A similar sum is used to calculate total number of susceptible genomes.

Immune clearance

Following pocapavir neutralization, immune clearance is applied after a specified number of replications, t_{imm}, via the survival function $d(t)$. For $t < t_{\mathrm{imm}}$, $d(t) = 1$. For $t \geq t_{\mathrm{imm}}$, survival is given by an exponential decay function,

$$d(t) = \mathrm{e}^{(-I_{\mathrm{init}}(t - t_{\mathrm{imm}}))},$$

where the initial immune sensitivity, I_{init}, is drawn from a lognormal distribution,

$$I_{\mathrm{init}} \sim \mathrm{Lognormal}(\xi, \tau^2).$$

The parameters governing I_{init} (t_{imm}, ξ and τ) and the host cell population size, γ, were inferred by maximizing the log-likelihood of observing simulation clearance times, given matched placebo clearance times from the pocapavir clinical trial reported by Collett et al.[11].

The virions that survive immune clearance and carry resistant genomes are represented by R_{imm}. This is found by binomially sampling r_{sum}:

$$R_{imm} \sim \text{Bin}(r_{sum}, d(t)).$$

Note, immune clearance is considered in the stochastic model only.

Initializing the next generation

In the stochastic model, draws from R_{imm} and S_{imm} represent the number of resistant and susceptible genomes that can infect cells in the next generation (that is, $r_{tot,t+1}$ and $s_{tot,t+1}$). If the realized values of $r_{tot,t+1}$ and $s_{tot,t+1}$ both equal zero, the simulation is terminated.

Variation in phenotypic dominance

To explore the impact of susceptible dominance over the resistant phenotype, we changed the drug neutralization function to simulate different relationships between resistant subunit composition and virion survival. Using the standard logistic function as our base, we used a steepness coefficient of $k = 100$ to simulate a step-like function, and varied i_0 to set the inflection point, corresponding to the minimum number of resistant subunits needed to render a virion phenotype resistant to drug. Otherwise, simulations were initialized with the same parameters as the pocapavir simulations.

Fitness cost of resistance

We examined fitness costs of resistance through a linear fitness function in which each additional resistant subunit in a capsid was associated with a κ decrease in virion extracellular survival probability, regardless of drug pressure ($\kappa \in [0, 0.0165]$; Extended Data Fig. 6). Unless otherwise noted, $\kappa = 0$.

Variation in drug strength

To explore the impact of drug strength on clinical outcomes, we scaled the original pocapavir fitness function such that

$$\omega'(i,t) = y_0' + \frac{(\omega(i,t) - y_0)(y_\sigma - y_0')}{y_\sigma - y_0},$$

where y_0 is the fitness of a fully susceptible capsid in the presence of pocapavir, y_σ is the fitness of a fully resistant capsid in the presence of pocapavir and y_0' is the new survival probability of a virion composed entirely of susceptible subunits. Otherwise, simulations were initialized with the same parameters as the pocapavir simulations.

Parameter inference

Parameters were inferred by numerical optimization in R (version 4.1.0)[52]. The specific objective functions varied by model and are described below.

Estimation of viral burst size. We inferred the effective viral burst size by fitting model outputs to mixed cell culture data from Tanner et al.[6], using matched initial MOIs. We specifically compared our simulated data with reported results of pure Mahoney strain PV with the VP3-A24V mutation in cell culture. This mutation is one of the most commonly observed in experiments selecting for resistance[9,10] and was the only strain/mutation pairing for which there was a negative control reported in Tanner et al.[6]. We evaluated model fit by minimizing the sum of squared differences between the log values of the observed and simulated plaque-forming units (PFU) after one round of replication. Specifically, we minimized

$$\sum_l (\log(\text{real\_pfu}_l) - \log(\text{sim\_pfu}_l))^2,$$

where l is the set of resistant MOI and susceptible MOI coinfected pairs reported by Tanner et al.[6]. Fitted values and their empirically measured comparisons are reported in Extended Data Table 1.

Estimation of immune clearance parameters. Parameters governing immune clearance and host cell population size were estimated by fitting a stochastic model of infection and clearance (assuming no drug effect; that is, $\omega(i,t) = 1$ for $i \in [0, 60], t \geq 0$ for all phenotypes at all timepoints) to placebo group clearance data from Collett et al.[11]. Because participants were not sampled daily, Collett et al. reported the clearance date as the first sample at which no virus was detected (Fig. 2). To replicate this, we rounded each simulated clearance time up to the next available sampling day, following the trial design.

We simulated 480 placebo recipients (10× the original sample size) and calculated the probability of clearance on each sampled day. These model-based probabilities were compared with the empirical distribution using a multinomial log-likelihood. Specifically, after adding a small pseudocount to avoid log-zero issues, we computed

$$\log L = \sum_x n_x \times \log p_x$$

where n_x is the number of placebo participants observed to clear on day x, and p_x is the model-derived probability of clearance on day x. If a simulated participant cleared after day 43 (the final sampling day), we could not compare this outcome with empirical data and instead returned a fixed log-likelihood value of 1,000 to penalize these parameter settings. Fitted values and their empirically measured comparisons are reported in Extended Data Table 1.

We note that the relevant in vivo cellular population size γ is not well described in the literature, and its fitted value in our optimization routine is sensitive to starting conditions, suggesting that it does not drive likelihoods. We present results with the fitted value of $\gamma = 37{,}041$ in the main text, as it broadly matches clearance outcomes in the treated group, with two additional γ values resulting from different optimization initial conditions in Extended Data Fig. 4. We further analytically characterize the dependence of the extinction probability on $\gamma \times \mu$ in the 'In vivo cellular population size' section in the Supplementary Materials and Methods and Supplementary Fig. 1.

A complete account of the model equations, parameter inference and simulation details is provided in the Supplementary Materials and Methods.

Reporting summary

Further information on research design is available in the Nature Portfolio Reporting Summary linked to this article.

Data availability

All data used for the analyses are available via Zenodo at https://doi.org/10.5281/zenodo.17458552 (ref. 54).

Code availability

Code for simulations, data analysis and data visualization is available via Zenodo at https://doi.org/10.5281/zenodo.17458552 (ref. 54).

References

1. Hansen, E., Karslake, J., Woods, R. J., Read, A. F. & Wood, K. B. Antibiotics can be used to contain drug-resistant bacteria by maintaining sufficiently large sensitive populations. *PLoS Biol.* **18**, e3000713 (2020).
2. Colijn, C. & Cohen, T. How competition governs whether moderate or aggressive treatment minimizes antibiotic resistance. *eLife* **4**, e10559 (2015).

3. Andino, R. & Domingo, E. Viral quasispecies. *Virology* **479–480**, 46–51 (2015).
4. Wilke, C. O. & Novella, I. S. Phenotypic mixing and hiding may contribute to memory in viral quasispecies. *BMC Microbiol.* **3**, 11 (2003).
5. Loverdo, C. & Lloyd-Smith, J. O. Inter-generational phenotypic mixing in viral evolution. *Evolution* **67**, 1815–1822 (2013).
6. Tanner, E. J. et al. Dominant drug targets suppress the emergence of antiviral resistance. *eLife* **3**, e03830 (2014).
7. Leeks, A. et al. Open questions in the social lives of viruses. *J. Evol. Biol.* **36**, 1551–1567 (2023).
8. Tanner, E. J., Kirkegaard, K. A. & Weinberger, L. S. Exploiting genetic interference for antiviral therapy. *PLoS Genet.* **12**, e1005986 (2016).
9. Kouiavskaia, D. V. et al. Immunological and pathogenic properties of poliovirus variants selected for resistance to antiviral drug V-073. *Antiviral Ther.* **16**, 999–1004 (2011).
10. Liu, H.-M. et al. Characterization of poliovirus variants selected for resistance to the antiviral compound V-073. *Antimicrob. Agents Chemother.* **56**, 5568–5574 (2012).
11. Collett, M. S. et al. Antiviral activity of pocapavir in a randomized, blinded, placebo-controlled human oral poliovirus vaccine challenge model. *J. Infect. Dis.* **215**, 335–343 (2017).
12. Copelyn, J. et al. Clearance of immunodeficiency-associated vaccine-derived poliovirus infection with pocapavir. *Pediatr. Infect. Dis. J.* **39**, 435 (2020).
13. Torres-Torres, S. et al. First use of investigational antiviral drug pocapavir (V-073) for treating neonatal enteroviral sepsis. *Pediatr. Infect. Dis. J.* **34**, 52 (2015).
14. Griffin, A. S. & Leeks, A. Exploiting social traits for clinical applications in bacteria and viruses. *npj Antimicrob. Resist.* **3**, 1–9 (2025).
15. Weinberger, L. S., Schaffer, D. V. & Arkin, A. P. Theoretical design of a gene therapy to prevent AIDS but not human immunodeficiency virus type 1 infection. *J. Virol.* **77**, 10028–10036 (2003).
16. Metzger, V. T., Lloyd-Smith, J. O. & Weinberger, L. S. Autonomous targeting of infectious superspreaders using engineered transmissible therapies. *PLoS Comput. Biol.* **7**, e1002015 (2011).
17. Pitchai, F. N. N. et al. Engineered deletions of HIV replicate conditionally to reduce disease in nonhuman primates. *Science* **385**, eadn5866 (2024).
18. Chaturvedi, S. et al. Identification of a therapeutic interfering particle—a single-dose SARS-CoV-2 antiviral intervention with a high barrier to resistance. *Cell* **184**, 6022–6036 (2021).
19. Chaturvedi, S. et al. A single-administration therapeutic interfering particle reduces SARS-CoV-2 viral shedding and pathogenesis in hamsters. *Proc. Natl Acad. Sci. USA* **119**, e2204624119 (2022).
20. Rezelj, V. V. et al. Defective viral genomes as therapeutic interfering particles against flavivirus infection in mammalian and mosquito hosts. *Nat. Commun.* **12**, 2290 (2021).
21. Zhang, L. et al. Adaptive therapy: a tumor therapy strategy based on Darwinian evolution theory. *Crit. Rev. Oncol. Hematol.* **192**, 104192 (2023).
22. Gatenby, R. A. & Brown, J. S. The evolution and ecology of resistance in cancer therapy. *Cold Spring Harbor Perspect. Med.* **10**, a040972 (2020).
23. Sicard, A., Michalakis, Y., Gutiérrez, S. & Blanc, S. The strange lifestyle of multipartite viruses. *PLoS Pathog.* **12**, e1005819 (2016).
24. Brooke, C. B. et al. Most influenza A virions fail to express at least one essential viral protein. *J. Virol.* **87**, 3155–3162 (2013).
25. Russell, A. B., Trapnell, C. & Bloom, J. D. Extreme heterogeneity of influenza virus infection in single cells. *eLife* **7**, e32303 (2018).
26. Romero, E. V. & Feder, A. F. Elevated HIV viral load is associated with higher recombination rate in vivo. *Mol. Biol. Evol.* **41**, msad260 (2024).
27. Schulte, M. B., Draghi, J. A., Plotkin, J. B. & Andino, R. Experimentally guided models reveal replication principles that shape the mutation distribution of RNA viruses. *eLife* **4**, e03753 (2015).
28. Schulte, M. B. & Andino, R. Single-cell analysis uncovers extensive biological noise in poliovirus replication. *J. Virol.* **88**, 6205–6212 (2014).
29. Mateo, R., Nagamine, C. M. & Kirkegaard, K. Suppression of drug resistance in dengue virus. *mBio* **6**, 01960–15 (2015).
30. Hunter, M. & Fusco, D. Superinfection exclusion: a viral strategy with short-term benefits and long-term drawbacks. *PLoS Comput. Biol.* **18**, e1010125 (2022).
31. Kerviel, A., Zhang, M. & Altan-Bonnet, N. A new infectious unit: extracellular vesicles carrying virus populations. *Annu. Rev. Cell Dev. Biol.* **37**, 171–197 (2021).
32. Chen, Y.-H. et al. Phosphatidylserine vesicles enable efficient en bloc transmission of enteroviruses. *Cell* **160**, 619–630 (2015).
33. Egger, D. & Bienz, K. Intracellular location and translocation of silent and active poliovirus replication complexes. *J. Gen. Virol.* **86**, 707–718 (2005).
34. Choppin, P. W. & Holmes, K. V. Replication of SV5 RNA and the effects of superinfection with poliovirus. *Virology* **33**, 442–451 (1967).
35. Aguilera, E. R., Erickson, A. K., Jesudhasan, P. R., Robinson, C. M. & Pfeiffer, J. K. Plaques formed by mutagenized viral populations have elevated coinfection frequencies. *mBio* **8**, 02020-16 (2017).
36. Erickson, A. K. et al. Bacteria facilitate enteric virus co-infection of mammalian cells and promote genetic recombination. *Cell Host Microbe* **23**, 77–88 (2018).
37. Freistadt, M. S., Kaplan, G. & Racaniello, V. R. Heterogeneous expression of poliovirus receptor-related proteins in human cells and tissues. *Mol. Cell. Biol.* **10**, 5700–5706 (1990).
38. Molfetta, R. et al. CD155: a multi-functional molecule in tumor progression. *Int. J. Mol. Sci.* **21**, 922 (2020).
39. Farrell, A., Phan, T., Brooke, C. B., Koelle, K. & Ke, R. Semi-infectious particles contribute substantially to influenza virus within-host dynamics when infection is dominated by spatial structure. *Virus Evol.* **9**, vead020 (2023).
40. Buontempo, P. J. et al. SCH 48973: a potent, broad-spectrum, antienterovirus compound. *Antimicrob. Agents Chemother.* **41**, 1220–1225 (1997).
41. Schlegel, A., Giddings, T. H., Ladinsky, M. S. & Kirkegaard, K. Cellular origin and ultrastructure of membranes induced during poliovirus infection. *J. Virol.* **70**, 6576–6588 (1996).
42. Novoa, R. R. et al. Virus factories: associations of cell organelles for viral replication and morphogenesis. *Biol. Cell* **97**, 147–172 (2005).
43. Dahmane, S. et al. Membrane-assisted assembly and selective secretory autophagy of enteroviruses. *Nat. Commun.* **13**, 5986 (2022).
44. Wilke, C. O. Quasispecies theory in the context of population genetics. *BMC Evol. Biol.* **5**, 44 (2005).
45. Santer, M. & Uecker, H. Evolutionary rescue and drug resistance on multicopy plasmids. *Genetics* **215**, 847–868 (2020).
46. Sun, L. et al. Effective polyploidy causes phenotypic delay and influences bacterial evolvability. *PLoS Biol.* **16**, e2004644 (2018).
47. DeLong, J. P. et al. Towards an integrative view of virus phenotypes. *Nat. Rev. Microbiol.* **20**, 83–94 (2022).
48. Yousaf, I. et al. Brain tropism acquisition: the spatial dynamics and evolution of a measles virus collective infectious unit that drove lethal subacute sclerosing panencephalitis. *PLoS Pathog.* **19**, e1011817 (2023).

49. Xue, K. S., Hooper, K. A., Ollodart, A. R., Dingens, A. S. & Bloom, J. D. Cooperation between distinct viral variants promotes growth of H3N2 influenza in cell culture. *eLife* **5**, e13974 (2016).
50. Shirogane, Y. et al. Collective fusion activity determines neurotropism of an en bloc transmitted enveloped virus. *Sci. Adv.* **9**, eadf3731 (2023).
51. Perales, C., Mateo, R., Mateu, M. G. & Domingo, E. Insights into RNA virus mutant spectrum and lethal mutagenesis events: replicative interference and complementation by multiple point mutants. *J. Mol. Biol.* **369**, 985–1000 (2007).
52. R Core Team. *R: A Language and Environment for Statistical Computing* (R Foundation for Statistical Computing, 2024).
53. Wickham, H. *ggplot2: Elegant Graphics for Data Analysis* (Springer, 2016); https://ggplot2.tidyverse.org
54. Robertson, A., Kerr, B. & Feder, A. federlab/polio-res-eco-evo: Initial release. *Zenodo* https://doi.org/10.5281/zenodo.17458552 (2025).

Acknowledgements

We thank Feder and Kerr lab members and two reviewers for useful project and manuscript feedback. We thank G. Thebaud for the helpful advice on fitting the pocapavir fitness function. This work was possible by funding from NIH training grant T32-GM136534-02 supporting A.J.R. and by the Environmental Biology Division from the National Science Foundation (grant number 2142718 to B.K.).

Author contributions

A.J.R., B.K. and A.F.F. contributed to study conceptualization and design. A.J.R. performed the analysis. A.J.R., B.K. and A.F.F. interpreted the results, wrote the original draft of the manuscript and contributed to review and editing of the manuscript.

Competing interests

The authors declare no competing interests.

Additional information

Extended data is available for this paper at https://doi.org/10.1038/s41559-025-02926-x.

Supplementary information The online version contains supplementary material available at https://doi.org/10.1038/s41559-025-02926-x.

Correspondence and requests for materials should be addressed to Benjamin Kerr or Alison F. Feder.

Peer review information *Nature Ecology & Evolution* thanks the anonymous reviewer(s) for their contribution to the peer review of this work.

https://doi.org/10.1038/s41559-025-02926-x

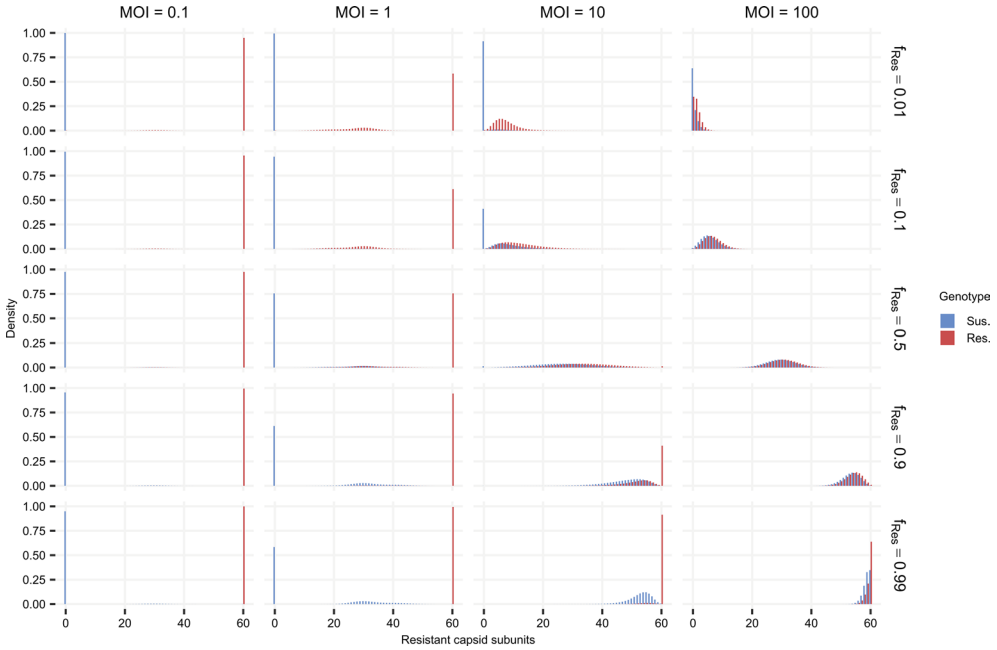

Extended Data Fig. 1 | Distribution of capsid subunit compositions following viral replication. For cellular populations infected by viruses with different frequencies of genotypic resistance ($f_{Res} \in \{0.01, 0.1, 0.5, 0.9, 0.99\}$, rows) and at different multiplicities of infection (MOI $\in \{0.1, 1, 10, 100\}$, columns), we plot the densities of virions emerging from these cells whose capsids contain different numbers of resistant capsid subunits. Outcomes are plotted separately based on if virions contain a susceptible genome (blue) or a resistant one (red). Simulations were run using standard model parameters reported in Extended Data Table 1. At low MOIs (0.1 and 1), progeny genomes are predominantly encapsidated in capsids reflecting their own genotype (that is, homogeneous capsids). At higher MOIs (10 and 100), progeny genomes are more frequently encapsidated in mixed capsids due to increased coinfection. Capsid composition is most mixed when resistant and susceptible genotypes are present at similar frequencies.

https://doi.org/10.1038/s41559-025-02926-x

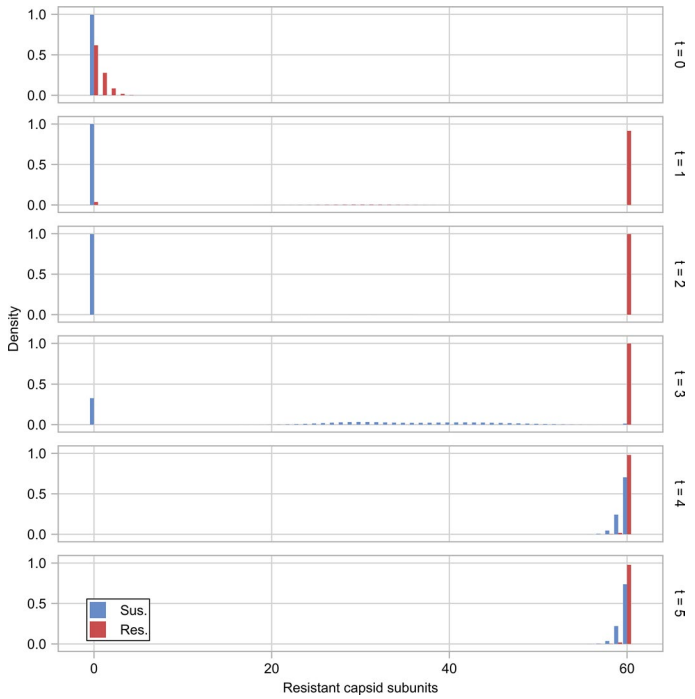

Extended Data Fig. 2 | Distribution of capsid subunit compositions over time in a serial passaging experiment. For each timestep in the serial passaging experiment shown in Fig. 4d (rows), we plot the density of capsid subunit compositions (that is, the number of resistant capsid subunits) for pre-neutralization virions based on whether they contain a susceptible (blue) or resistant (red) genome. The population was initialized with $f_{Res} = 10^{-4}$ and an MOI of 100. At $t = 0$, both resistant and susceptible genomes are packaged in highly susceptible capsids, but as the MOI drops, resistant and susceptible genomes are increasingly packaged in capsids matching their phenotypes. While MOI remains low and susceptible genomes become increasingly rare ($t = 3$), the phenotypic variance of susceptible genomes becomes large based on whether or not they coinfect with resistant ones. After rebound ($t \geq 4$), both resistant and susceptible genomes are packaged in highly resistant capsids.

https://doi.org/10.1038/s41559-025-02926-x

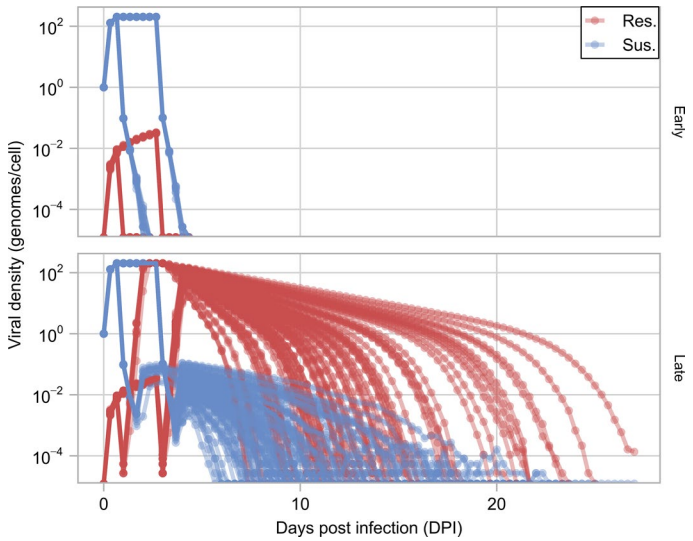

Extended Data Fig. 3 | Population dynamics of individual simulations in the simulated pocapavir clinical trial. For each simulated viral population in the pocapavir clinical trial summarized in Fig. 4f, we plot the viral density (genomes/cell) for resistant (red) and susceptible (blue) genomes over time. We stratify populations into early clearers (top) or late clearers (bottom) based on if the clearance time was earlier that 7 days post infection (DPI) or later than or equal to 7 DPI. As in the clinical trial, simulations were administered pocapavir beginning either 24 or 72 hours post infection, which causes the two asynchronous drops in viral density 1 and 3 days post infection.

https://doi.org/10.1038/s41559-025-02926-x

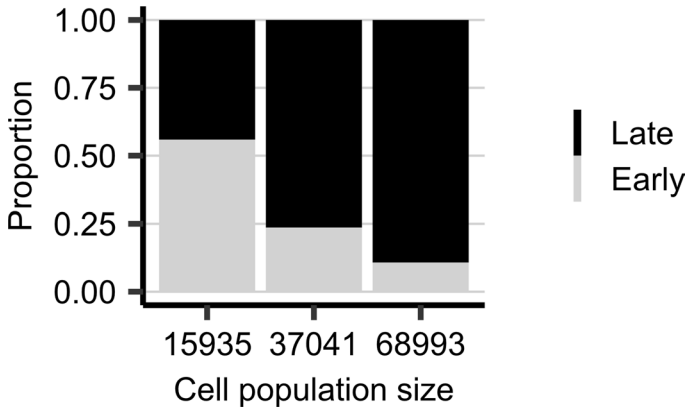

Extended Data Fig. 4 | Smaller host cell population sizes lead to more frequent early clearance in simulated clinical trials. Immune clearance parameters were optimized starting from three different initial host cell population sizes (15,000, 30,000, and 60,000) and converged to values similar to their starting conditions (15,935, 37,041, and 68,992, respectively). The frequency of early (< 7 days, black) versus late (≥7 days, grey) clearance was dependent on host cell population size, where early clearance was more common in simulations with smaller host cell population sizes (n = 93 simulations). In the main text, results are shown with the intermediate initial conditions (γ = 37, 041).

https://doi.org/10.1038/s41559-025-02926-x

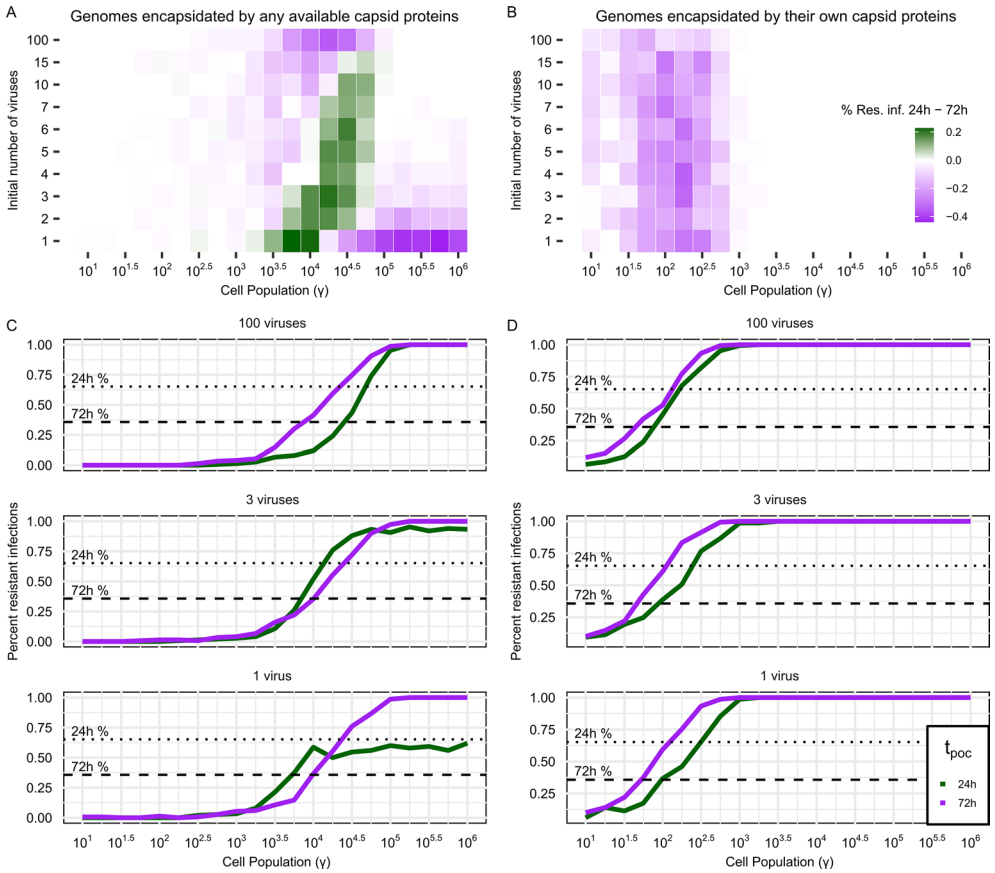

Extended Data Fig. 5 | Intracellular protein sharing can increase the frequency of resistance evolution during early treatment. Collett et al.[11] found that a greater proportion of viral populations treated 24 hours post-infection developed resistance than those treated 72 hours post- infection (15/23 versus 25/70; $p = 0.0163$, Fisher's exact test). We examined the emergence of this behaviour using the model in this manuscript (in which genomes can be encapsidated by any available intracellular capsid proteins), and a model without intra-cellular mixing (in which genomes are encapsidated only by capsid proteins corresponding to their genotype). (**A**, **B**) We compared the rates of resistance evolution in the 24 and 72 hour treatment groups across host cell population sizes (γ) and initial numbers of infecting susceptible viruses (n = 150 per group and parameter set, $f_{Res} \geq 50\%$ defined as resistant). We identified conditions in which earlier treatment was associated with more resistance evolution in the 24 hour treatment group than the 72 hour treatment group (shown in green) in the intra-cellular mixing model (**A**) but not the non-mixing model (**B**). (**C**-**D**) Example rows from (**A**) and (**B**) show the proportion of resistant infections in the 24 hour (green) versus 72 hour (purple) treatment groups under example initial conditions. Clinical resistance frequencies from Collett et al.[11] at the 24 hour and 72 hour treatment times are shown as dotted and dashed lines, respectively.

https://doi.org/10.1038/s41559-025-02926-x

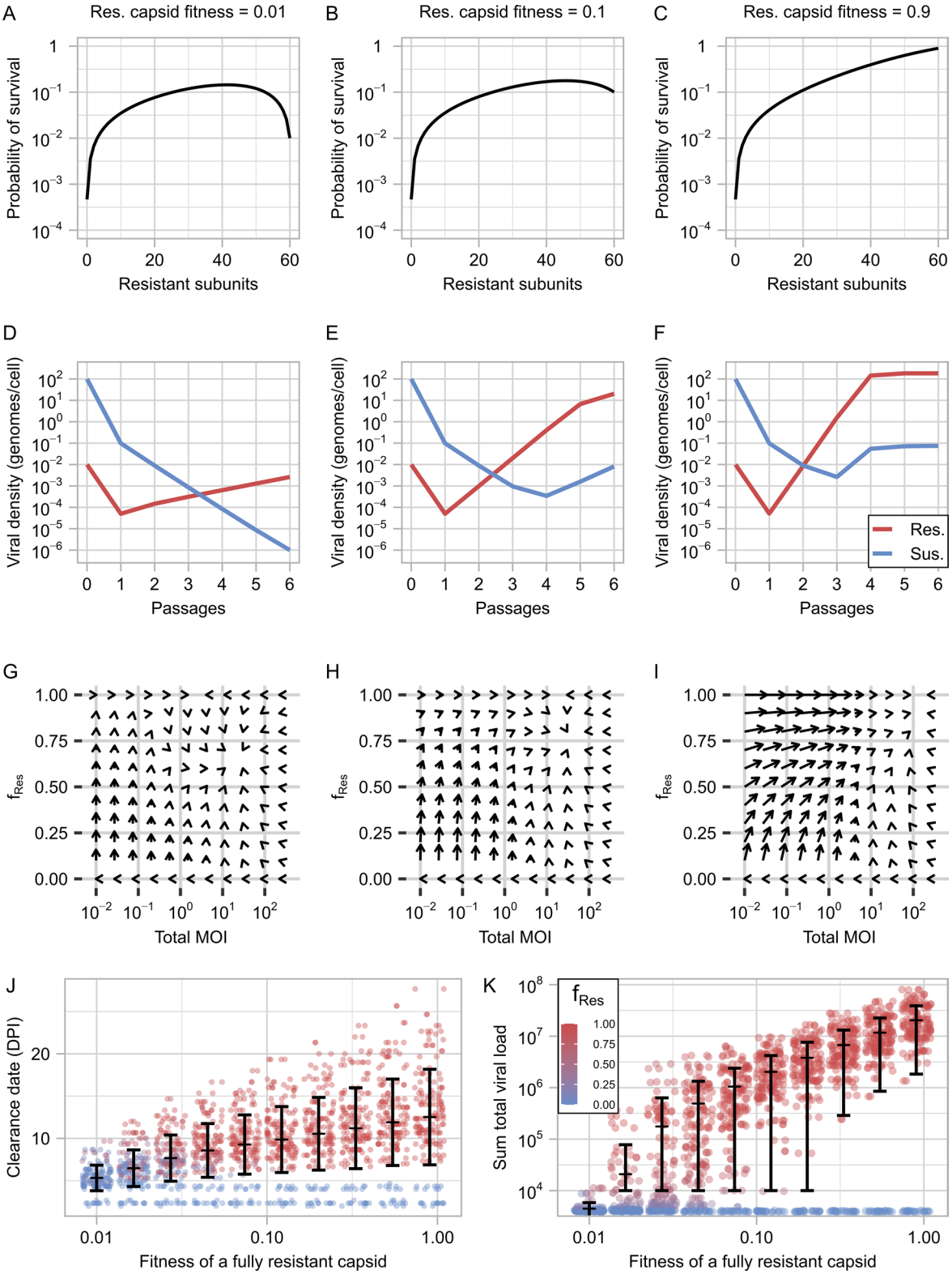

Extended Data Fig. 6 | Fitness cost of phenotypic resistance impairs the spread of resistance and results in more favorable clinical outcomes. (**A-C**) We generated compound fitness curves that accounted for both the standard fitness cost imposed by pocapavir and a linear fitness cost associated with greater numbers of resistant subunits per virion. The fitness of a fully resistant capsid is noted above its respective curve. Deterministic model simulations using the fitness functions in **A-C** reveal that greater costs of resistance slow the rate of resistance evolution and reduce viral densities over 6 passages (initial MOI = 100, initial $f_{Res} = 10^{-4}$, **D-F**) and reduce the equilibrium values of both total MOI and f_{Res} (**G-I**). Clinical trials simulated with the same immune parameters and pocapavir treatment times as in Fig. 4f, but incorporating fitness costs ($\kappa \in [0, 0.0165]$), showed earlier average clearance (**J**), reduced total viral loads (**K**), and lower resistance frequencies (f_{Res}; legend in **K** applies to point colours in **J**; horizontal line indicates mean value, bars show ± standard deviation).

https://doi.org/10.1038/s41559-025-02926-x

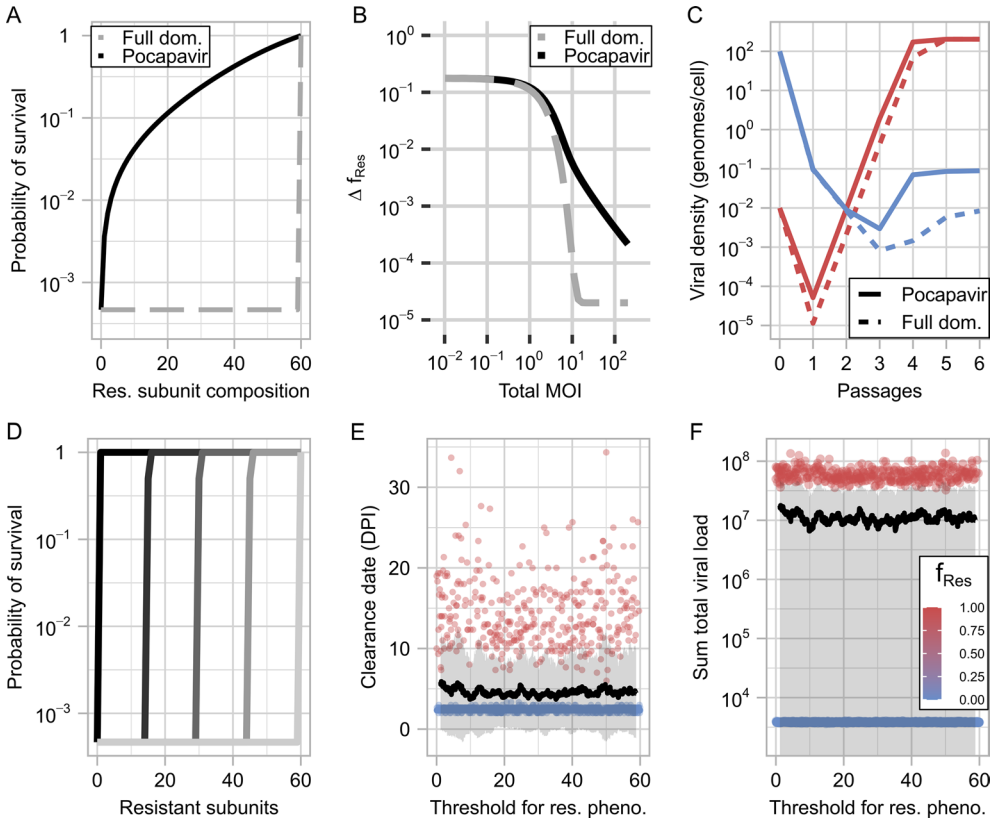

Extended Data Fig. 7 | More 'dominant' drugs do not suppress resistance better than pocapavir. (**A**) We considered a hypothetical drug to which drug resistant capsid subunits only conferred a survival advantage if all 60 subunits were resistant (that is, susceptible subunits fully dominate resistant ones). We compared this fully dominant drug (dashed grey) to pocapavir (solid black). (**B**) In single passage simulations assessing the change in resistance frequency (Δf_{Res}) as a function of the initial MOI, the fully dominant drug suppressed resistance marginally better than pocapavir at high MOI (initial $f_{Res} = 10^{-4}$). (**C**) However, in a deterministic serial passage experiment, both drugs (pocapavir, solid; the fully dominant drug, dashed) led to similar population trajectories for susceptible and resistant viral densities over time. In (**A**-**C**), we considered that a capsid must have 60 resistant subunits to have any increased survival probability. We next consider how lowering that threshold to generate a resistance response (that is, 100% survival probability when treated with pocapavir) from 60 affects clinical outcomes. Five such thresholds are plotted in (**D**), but 2000 trials were run across a range of threshold values. Threshold values do not affect clearance date (**E**) or sum total viral load over the course of infection (**F**). Each point represents an individual simulation with a given resistant capsid threshold value to confer resistance, and points are coloured by the frequency of genotypic resistance observed in the simulation over the course of infection. For both (**E**) and (**F**), the black line shows a rolling mean and the grey ribbon shows the variance around the mean.

https://doi.org/10.1038/s41559-025-02926-x

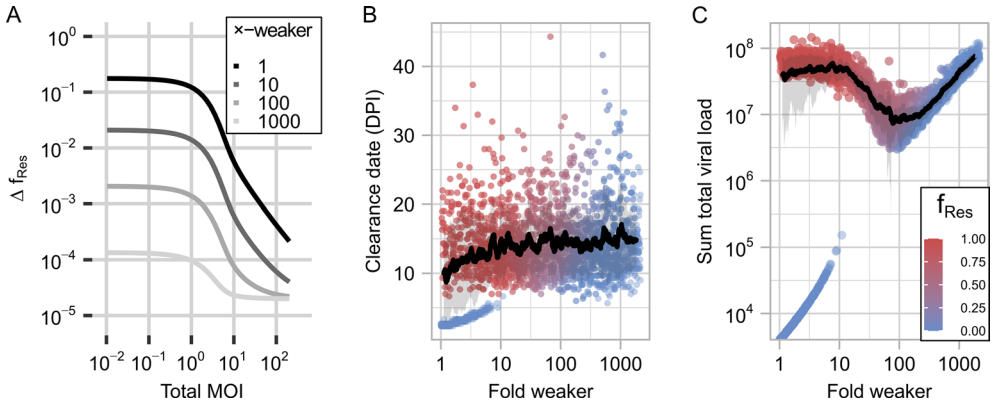

Extended Data Fig. 8 | Reducing drug potency lowers selection for resistance and can maintain lower viral loads over time. (**A**) In single passage simulations assessing the change in resistance frequency (Δf_{Res}) as a function of the initial MOI, less potent drugs (10×, 100×, 1000× weaker) led to smaller increases in the frequency of resistance than pocapavir (initial $f_{Res} = 10^{-4}$). Note, clinical trial outcomes for these specific drugs are plotted in Fig. 5. We also ran 2000 clinical simulations exploring drugs with a range of potency reductions between 1× and 2147× weaker. (**B**) Drugs weaker than pocapavir had later clearance times due to the reduced probability of population bottlenecks leading to early extinction. (**C**) However, we observed a non-monotonic relationship between drug weakness and the sum total viral load, in which drugs with intermediate weakness (≈100× weaker) best reduce sum total viral load. For both (**B**) and (**C**), each point represents an individual simulation with a given resistant capsid threshold value to confer resistance, and points are coloured by the frequency of genotypic resistance observed in the simulation over the course of infection (legend in (**C**)). The black line shows a rolling mean and the grey ribbon shows the variance around the mean.

https://doi.org/10.1038/s41559-025-02926-x

Extended Data Table 1 | Estimated model parameters and their associated notation, estimated values and empirical comparisons

Parameter (units)	Variable	Estimated Value	Empirical Comparison
Fitness function, steepness	k	0.061675	-
Fitness function, inflection	i_0	60	-
Effective burst size (infections particles/cell)	β	203.17	23.89 - 277.78 (particles/cell[2, 3] × PFU/particle [4])
Clinical model, host cell pop. (cells)	γ	$37,041$	-
Imm. clearance delay (hours)	t_{imm}	80	72 to 125 [5]
Imm. clearance distribution, mean	ξ	-1.424	-
Imm. clearance distribution, SD	τ	0.460	-

Parameter estimates were obtained by fitting the model to cell culture and clinical trial data. In brief, burst size and fitness function parameters were estimated by fitting to cell culture data reported in Tanner et al.[6], and host cell population and immune clearance parameters were estimated by fitting to clinical data from a placebo-treated group reported by Collett et al.[11] (see 'Parameter inference' in the Methods).

nature portfolio

Corresponding author(s): Benjamin Kerr, Alison Feder

Last updated by author(s): Sep 26, 2025

Reporting Summary

Nature Portfolio wishes to improve the reproducibility of the work that we publish. This form provides structure for consistency and transparency in reporting. For further information on Nature Portfolio policies, see our Editorial Policies and the Editorial Policy Checklist.

Statistics

For all statistical analyses, confirm that the following items are present in the figure legend, table legend, main text, or Methods section.

n/a	Confirmed
☐	☒ The exact sample size (*n*) for each experimental group/condition, given as a discrete number and unit of measurement
☐	☒ A statement on whether measurements were taken from distinct samples or whether the same sample was measured repeatedly
☐	☒ The statistical test(s) used AND whether they are one- or two-sided *Only common tests should be described solely by name; describe more complex techniques in the Methods section.*
☐	☒ A description of all covariates tested
☐	☒ A description of any assumptions or corrections, such as tests of normality and adjustment for multiple comparisons
☐	☒ A full description of the statistical parameters including central tendency (e.g. means) or other basic estimates (e.g. regression coefficient) AND variation (e.g. standard deviation) or associated estimates of uncertainty (e.g. confidence intervals)
☐	☒ For null hypothesis testing, the test statistic (e.g. *F*, *t*, *r*) with confidence intervals, effect sizes, degrees of freedom and *P* value noted *Give P values as exact values whenever suitable.*
☒	☐ For Bayesian analysis, information on the choice of priors and Markov chain Monte Carlo settings
☐	☒ For hierarchical and complex designs, identification of the appropriate level for tests and full reporting of outcomes
☒	☐ Estimates of effect sizes (e.g. Cohen's *d*, Pearson's *r*), indicating how they were calculated

Our web collection on statistics for biologists contains articles on many of the points above.

Software and code

Policy information about availability of computer code

Data collection	All data were generated using R version 4.1.0. The code used to generate data from our deterministic and stochastic models are available at https://github.com/federlab/polio-res-eco-evo/scr.
Data analysis	All data were analyzed using R version 4.1.0. All code for our analyses can be found at https://github.com/federlab/polio-res-eco-evo/scr. A snakemake pipeline in the home directory of this GitHub repository was used to run the reported analyses. All code used to generate figures can be found at https://github.com/federlab/polio-res-eco-evo/scr/panels.

For manuscripts utilizing custom algorithms or software that are central to the research but not yet described in published literature, software must be made available to editors and reviewers. We strongly encourage code deposition in a community repository (e.g. GitHub). See the Nature Portfolio guidelines for submitting code & software for further information.

Data

Policy information about availability of data

All manuscripts must include a data availability statement. This statement should provide the following information, where applicable:

- Accession codes, unique identifiers, or web links for publicly available datasets
- A description of any restrictions on data availability
- For clinical datasets or third party data, please ensure that the statement adheres to our policy

All data used for, and generated by this project can be found at https://github.com/federlab/polio-res-eco-evo. We compared our model results to data produced

by Tanner et al., eLife (2014), and Collett et al., JID (2016), all raw data can be found at https://github.com/federlab/polio-res-eco-evo/dat/. Clinical trial data is de-identified, with individual infection durations being reported. All new data generated for our analyses reported in the manuscript can be found at https://github.com/federlab/polio-res-eco-evo/runs/ddt_logistic_mu_2e-05_2025-09-02/dat_gen/, or at the request of the author.

Research involving human participants, their data, or biological material

Policy information about studies with human participants or human data. See also policy information about sex, gender (identity/presentation), and sexual orientation and race, ethnicity and racism.

Reporting on sex and gender	N/A
Reporting on race, ethnicity, or other socially relevant groupings	N/A
Population characteristics	N/A
Recruitment	N/A
Ethics oversight	N/A

Note that full information on the approval of the study protocol must also be provided in the manuscript.

Field-specific reporting

Please select the one below that is the best fit for your research. If you are not sure, read the appropriate sections before making your selection.

☐ Life sciences ☐ Behavioural & social sciences ☒ Ecological, evolutionary & environmental sciences

For a reference copy of the document with all sections, see nature.com/documents/nr-reporting-summary-flat.pdf

Ecological, evolutionary & environmental sciences study design

All studies must disclose on these points even when the disclosure is negative.

Study description	In this study, we developed an evolutionary model to explore the interaction between polioviruses resistant or susceptible to the antiviral pocapavir. We compared our simulation data with previously published cell culture data, and clinical trial data. We first developed a basic form of the model which could replicate results derived from cell culture experiments. We then expanded on our model to try to replicate intrahost evolution, which we compared to clinical trial outcomes. For large-scale analyses in which we looked for general trends using the stochastic model, we used ~10,000 simulations to explore the particular parameter space.
Research sample	Our research was computational and simulation based, therefore we did not have a live research sample. We did, however, compare our results to previously published clinical trial data, and previously reported cell culture data (Tanner et al., eLife (2014), and Collett et al., JID (2016)), and note when we do so.
Sampling strategy	For deterministic models, sample size is not relevant. For stochastic models, we ran as many replicates as computationally feasible, generally on the order of 100-10,000 simulations per in silico experiment. We verified that our sample sizes were sufficient by using different initial seeds, comparing our results across experiments (data not show in our manuscript).
Data collection	Data was generated using R 4.1.0 by A.J.R. All scripts used to generate, analyze and plot the data can be found at https://github.com/federlab/polio-res-eco-evo.
Timing and spatial scale	N/A
Data exclusions	No data were excluded from the analysis.
Reproducibility	A snakemake pipeline was designed to easily re-run all simulations and analysis, which is highly reproducible. We verified the reproducibility of our results by using different initial seeds for our stochastic simulations, and by varying parameter values. Our results were robust to this testing, and can be reproduced by the code at https://github.com/federlab/polio-res-eco-evo.
Randomization	N/A
Blinding	The investigators were not blinded during this study as all results were generated by simulations and not subjective.

Did the study involve field work? ☐ Yes ☒ No

Reporting for specific materials, systems and methods

We require information from authors about some types of materials, experimental systems and methods used in many studies. Here, indicate whether each material, system or method listed is relevant to your study. If you are not sure if a list item applies to your research, read the appropriate section before selecting a response.

Materials & experimental systems

n/a	Involved in the study
☒	☐ Antibodies
☒	☐ Eukaryotic cell lines
☒	☐ Palaeontology and archaeology
☒	☐ Animals and other organisms
☒	☐ Clinical data
☒	☐ Dual use research of concern
☒	☐ Plants

Methods

n/a	Involved in the study
☒	☐ ChIP-seq
☒	☐ Flow cytometry
☒	☐ MRI-based neuroimaging

Plants

Seed stocks	N/A
Novel plant genotypes	N/A
Authentication	N/A